

# Mass spectral characterization of secondary organic aerosol from urban cooking and vehicular sources

Wenfei Zhu<sup>1</sup>, Song Guo<sup>1,2\*</sup>, Zirui Zhang<sup>1</sup>, Hui Wang<sup>1</sup>, Ying Yu<sup>1</sup>, Zheng Chen<sup>1</sup>, Ruizhe Shen<sup>1</sup>, Rui Tan<sup>1</sup>, Kai Song<sup>1</sup>, Kefan Liu<sup>1</sup>, Rongzhi Tang<sup>1</sup>, Yi Liu<sup>1</sup>, Shengrong Lou<sup>3</sup>, Yuanju Li<sup>1</sup>, Wenbin Zhang<sup>4</sup>, Zhou Zhang<sup>4</sup>, Shijin Shuai<sup>4</sup>, Hongming Xu<sup>4</sup>, Shuangde Li<sup>5</sup>, Yunfa Chen<sup>5</sup>, Min Hu<sup>1</sup>, Francesco Canonaco<sup>6</sup>, Andre. S. H. Prévôt<sup>6</sup>

<sup>1</sup> State Key Joint Laboratory of Environmental Simulation and Pollution Control, International Joint Laboratory for Regional Pollution Control, Ministry of Education (IJRC), College of Environmental Sciences and Engineering, Peking University, Beijing 100871, China P. R.

<sup>2</sup> Collaborative Innovation Center of Atmospheric Environment and Equipment Technology, Nanjing University of Information Science & Technology, Nanjing 210044, China P. R.

<sup>3</sup> State Environmental Protection Key Laboratory of Formation of Urban Air Pollution Complex, Shanghai Academy of Environmental Sciences, Shanghai 200233, China P. R.

<sup>4</sup> State Key Laboratory of Automotive Safety and Energy, Tsinghua University, Beijing 100084, China P. R.

<sup>5</sup> State Key Laboratory of Multiphase Complex Systems, Institute of Process Engineering, Chinese Academy of Sciences, Beijing 100190, China P. R.

<sup>6</sup> Laboratory of Atmospheric Chemistry, Paul Scherrer Institute (PSI), Villigen 5232, Switzerland

Corresponding authors:

\*Song Guo – State Key Joint Laboratory of Environmental Simulation and Pollution Control, College of Environmental Sciences and Engineering, Peking University, Beijing 100871, China P. R.; Email: songguo@pku.edu.cn

**Abstract** In the present work, we conducted experiments of secondary organic aerosol (SOA) formation from urban cooking and vehicular sources to characterize the mass spectral features of primary organic aerosol (POA) and SOA using an high-resolution time-of-flight aerosol mass spectrometer (HR-ToF-AMS). Our results showed that the cooking styles have a greater impact on aged COA mass spectra than oxidation conditions. However, the oxidation conditions affect the aged HOA spectra more significantly than vehicle operating conditions. In our study, we use mass spectra similarity analysis and positive matrix factorization (PMF) analysis to establish the POA and SOA mass spectra of these two sources.

30 These mass spectra are used as source constraints in a multilinear engine (ME-2) model to apportion the OA sources in the  
31 atmosphere. Comparing with the traditional ambient PMF results, the improved ME-2 model can better quantify the  
32 contribution of POA and SOA from cooking and vehicular sources. Our work, for the first time, establishes the vehicle and  
33 cooking SOA source profiles, and can be further used in the OA source apportionment in the ambient atmosphere.

## 35 **1. Introduction**

36 Organic aerosol (OA) is an important component of fine particulate matter and has significant  
37 environmental and health effects, especially in urban areas (Guo et al., 2012; Guo et al., 2014; Ying et al.,  
38 2020). Currently, real-time measurements of OA based on the aerosol mass spectrometer (AMS) has become  
39 an effective way to explore OA characteristics in the field campaigns and laboratory studies (Canagaratna et  
40 al., 2007; Ge et al., 2017; Hu et al., 2016a; Huang et al., 2011; Kim et al., 2017; Li et al., 2017; Sun et al.,  
41 2016; Zhang et al., 2011). Applying positive matrix factorization (PMF) and a multilinear engine (ME-2)  
42 (Paatero, 1999) to analyze the high-resolution mass spectrometry fragments, OA can be further identified as  
43 primary organic aerosol (POA) and secondary organic aerosol (SOA). POA includes a kind of  
44 hydrocarbon-like OA, (HOA), cooking (COA), and biomass burning (BBOA), which SOA includes low  
45 oxygenated OA (LO-OOA) and more oxygenated OA (MO-OOA)(Canonaco et al., 2013; Elser et al., 2016;  
46 Qin et al., 2017; Zhang et al., 2017a; Zhou et al., 2018). Many previous studies have been found that HOA is  
47 mainly associated with vehicle-related emissions in the urban atmosphere (Hu et al., 2017; Xu et al., 2016;  
48 Zhang et al., 2017a). Hereinafter, HOA will be referred to as the abbreviation for organic aerosol emitted by  
49 urban vehicles. As lifestyle sources in urban, cooking and vehicular sources, that is COA and HOA mostly  
50 determine ambient OA loadings. For example, primary cooking OA (COA) and vehicle exhaust OA (HOA)  
51 accounted for 10-35 % and 6-26% of OA, respectively, in urban areas in China (He et al., 2011; Hu et al.,  
52 2017; Sun et al., 2010; Sun et al., 2014; Sun et al., 2018; Wang et al., 2016; Xu et al., 2016; Zhang et al.,

2014).

Besides the contribution to POA, many studies have found that cooking and vehicular sources may also emit a large number of volatile organic compounds (VOCs) (Gentner et al., 2009; Katragadda et al., 2010; Klein et al., 2016), semi-volatile organic compounds (SVOCs), and intermediate volatile organic compounds (IVOCs) ( $\geq C_{13}$ n-alkanes and fatty acids) (Louvaris et al., 2017; Schauer et al., 2002; Tang et al., 2021), which may also play important roles in SOA formation (Wang et al., 2021; Yu et al., 2021). However, based on collocated AMS measurements and factor analysis results, the SOA formed by vehicle and cooking sources cannot be effectively resolved from the total SOA due to the lack of secondary mass spectral profiles. The POA mass spectral profiles based on AMS including HOA (Collier et al., 2015), BBOA (Alfarra et al., 2007; He et al., 2010; Xu et al., 2020), and COA (He et al., 2010; Liu et al., 2017; Mohr et al., 2012; Xu et al., 2020) have been fully explored in laboratory studies and applied as constraint factors into the ME-2 model in the ambient air. Some studies have made it possible to quantify biogenic secondary aerosol products of a single precursor, such as isoprene oxidation products (IEPOX) (Budisulistiorini et al., 2013; Hu et al., 2016b), and have been extended to the urban atmosphere to obtain an IEPOX-SOA factor via PMF analysis of OA spectra (Zhang et al., 2017b). Although several studies explored the mass spectral characteristics of SOA from cooking and vehicular sources, i.e., heated cooking oils, gasoline motors, and diesel engines (Kaltsonoudis et al., 2017; Kroll et al., 2012; Liu et al., 2018; Presto et al., 2014), the spectral profiles of cooking SOA under actual cooking conditions and vehicle SOA under different emission conditions are still uncertain. Besides, to date, studies that used ME-2 for a better anthropogenic SOA source apportionment by inputting their SOA spectra as constraints remain scarce. Therefore, the mass spectra of SOA from abundant cooking and vehicular sources are urgent to characterize for conducting to acquire a better source apportionment of SOA.

In this study, cooking and vehicle experiments were carried out to investigate the variation in POA and

76 SOA spectra profiles emitted from vehicle emissions under different running conditions, and Chinese  
77 cooking emissions under different cooking styles using high-resolution time-of-flight AMS (HR-ToF-AMS).  
78 The mass spectral characterizations of POA and SOA from cooking and vehicle emissions were  
79 intercompared, and their changes in some indicated ionic fragments were elucidated. Besides, we verified  
80 the mass spectral profiles by applying POA and SOA profiles to ME-2 for source apportionment of OA in  
81 the winter observation with various primary emissions and the summer observation with high oxidation  
82 conditions.

## 83 **2. Materials and Methods**

### 84 **2.1 Simulation of POA emission and SOA formation from cooking and vehicular sources.**

85 For cooking, we prepared four dishes including deep-frying chicken, shallow-frying tofu, stir-frying  
86 cabbage, and Kung Pao chicken. The total cooking time for each experiment ranged from 40 to 66 min,  
87 which was almost related to the features of each dish (**Table S1**). Each dish was continuously carried out 8  
88 times in parallel during the cooking process until the closed kitchen was full of fumes. The fumes produced  
89 by cooking were introduced through the pipeline from the kitchen into the Gothenburg Potential Aerosol  
90 Mass (Go: PAM) reactor (Li et al., 2019) in the laboratory after being diluted 8 times by a Dekati Dilutor  
91 (e-Diluter, Dekati Ltd., Finland). Heat insulation cotton was wrapped around the sampling pipelines to  
92 prevent fumes from condensing on the wall of the pipe. We considered the emissions sampled after Go:  
93 PAM without OH radical as primary emissions, and those monitoring after Go: PAM with given OH radicals  
94 as secondary formation. The sampling time ranged from 58 to 90 min. In addition, the background blank  
95 groups and the dilution gas blank groups were separately completed using boiling water and dilution gas,  
96 according to the same steps as experimental groups. More information on the experimental setup of cooking  
97 simulations has been given in Zhang et al., 2020.

98 For vehicle, experiments were performed by using a Gasoline direct engine (GDI) with a commercial

99 China V gasoline fuel (Emission: 998cc; Maximum power: 100KW 6000rpm; Peak torque: 205Nm  
100 2000-3000rpm). Vehicle operating under real-life conditions were dynamic rotating speed-torque  
101 combination. For example, the combination of 1500 rpm rotating speed and 16Nm torque and 2000rpm  
102 rotating speed and 16Nm torque for the engine in this study reflect the realistic vehicle speed of 20km/h and  
103 40km/h, respectively. Five running conditions covering different speeds and torques, including  
104 1500rpm\_16Nm, 1750rpm\_16Nm, 2000rpm\_16Nm, 2000rpm\_32Nm, and 2000rpm\_40Nm, were used to  
105 characterize their POA and SOA mass spectra in this study. Once the engine warmed up, it continued to  
106 work under one running condition. After the three-way catalytic system, the exhaust from the engine tailpipe  
107 was diluted 30 times by the same dilution system for the cooking experiment. Then the diluted exhaust  
108 entered the Go: PAM through the stainless pipe wrapped by heat insulation cotton. For each running  
109 condition, five parallel experiments were conducted (**Table S2**). The sampling time was about 60 min for  
110 each experiment.

111 Go: PAM reactor consists of quartz tube that is 100 cm long and 9.6 cm in diameter, as described in  
112 Watne et al., 2018. The OH radicals in Go: PAM reactor is generated by the photolysis of ozone and the  
113 reaction in the presence of water vapor. We adjusted input ozone concentrations ranging from ~0 to ~6.5  
114 ppm and ~0 to ~4.0 ppm to change the OH radicals in the Go: PAM for vehicle and cooking experiments,  
115 respectively. The temperature, relative humidity, and the sampling residence time in Go: PAM for vehicle  
116 and cooking experiments were documented in the supplement material (**Table S3**).

## 117 **2.2 Instrumentation and data analysis.**

118 The design drawing on vehicle and cooking experiments is presented in **Figure S1**. Two scanning  
119 mobility particle sizers (SMPS; TSI Incorporation, USA) were set at the inlet and outlet of Go: PAM to  
120 correct the wall loss (Zhang et al., 2020). The size distribution and number concentration of particles were  
121 scanned every 2 (cooking) - 5 min (vehicle) before and after Go: PAM for cooking and vehicle experiment,

122 respectively. The mass concentrations of non-refractory submicron aerosol (NR-PM<sub>1</sub>), and high-resolution  
123 ions fragments of OA were recorded by HR-ToF-AMS (Aerodyne Research Incorporation, USA),  
124 synchronize with SMPS.

125 Before and after the two experiments, the ionization efficiency (IE) of HR-ToF-AMS was calibrated by  
126 applying 300 nm mono-dispersed ammonium nitrate particles synchronization with SMPS. The collection  
127 efficiency (CE) was obtained from comparing AMS and synchronous SMPS real-time measurement of  
128 particle mass concentrations at the outlet of Go: PAM. Besides, the real-time measurements of CO<sub>2</sub>  
129 concentrations (Model 410i, Thermo Electron Corporation, USA) were used to correct the influence of CO<sub>2</sub>  
130 on OA ion fragments, refer to (Canagaratna et al., 2015). Other gas phase measurements included carbon  
131 monoxide (CO, Thermo, Model 48i TL), NO<sub>x</sub> (Thermo, Model 42i TL), and SO<sub>2</sub> (Thermo, Model 42i TL).

132 The mass concentration, size distribution, and the ion-specified mass spectra of NR-PM<sub>1</sub> species were  
133 analyzed using the HR-ToF-AMS standard data analysis software (SQUIRREL version 1.57 and PIKA  
134 version 1.16). The elemental compositions (O/C, H/C, N/C, and OM/OC) were estimated by the  
135 “improved-ambient” updated method (Canagaratna et al., 2015). The OH exposure and equivalent  
136 photochemical age (EPA) were calculated by off-line methods according to SO<sub>2</sub> decay shown in Zhang et al.,  
137 2020, which were validated by a flow reactor exposure estimator using measured concentrations of reactive  
138 compounds such as VOCs, CO, and NO<sub>x</sub> (Peng et al., 2016). The OH exposure and photochemical age for  
139 all conditions in cooking and vehicle experiments were listed in **Table S3**.

### 140 **2.3 OA source apportionment**

141 The PMF model can describe the variability of a multivariate database as a linear combination of static  
142 factor profiles and their corresponding time series (Huang et al., 2020; Wang et al., 2017; Zhu et al., 2018).  
143 In this study, we used the Igor-based PMF model with PMF2.exe algorithm (Paatero and Hopke, 2003) and  
144 the PMF Evaluation Toolkit version 2.08D (Ulbrich et al., 2009) to split POA and SOA factors from cooking

145 and vehicle aged OA. The PMF model was also used to identify the source of OA for ambient atmosphere  
146 during the summer and winter observations of Shanghai, following the procedure presented in the literature  
147 (Hu et al., 2016a; Zhang et al., 2011), as described in section 3.3. In contrast to an unconstrained PMF  
148 analysis, ME-2 algorithm allows the user to add prior information (e.g., source profiles) into the model to  
149 constrain the matrix rotation and separated the mixed solution. In this study, we adopted the toolkit SoFi  
150 (Source Finder) with an a-value approach to perform organic HR-AMS datasets collected in Shanghai. The  
151 a-value can vary between 0 and 1, which is the extent to which the output profiles can vary from the model  
152 inputs. The a-value test was performed following the technical guidelines presented in Crippa et al., 2014.  
153 The reference mass spectral profiles that constrained in ME-2 analysis were derived from lab-based primary  
154 and secondary cooking and vehicular factors of this study. Details of the algorithm could refer to previous  
155 studies (Canonaco et al., 2013; Huang et al., 2020; Reyes-Villegas et al., 2016).

## 156 **2.4 Mass spectra similarity analysis.**

157 In this study, the angle  $\theta$  was used to evaluate the correlation between the two AMS mass spectra  
158 features. The angle  $\theta$  between the two AMS mass spectra (MSa, MSb) is given by:

$$159 \cos \theta = \frac{MSaMSb}{|MSa||MSb|}$$

160 The  $\theta$  angle between two mass spectra is 0-5, 5-10, 10-15, 15-30, and  $> 30$ , which means excellent  
161 consistency, good consistency, many similarities, limited similarities, and poor consistency, respectively  
162 (Kaltsonoudis et al., 2017; Kostenidou et al., 2009).

## 163 **3. Results and Discussion**

### 164 **3.1 Mass spectra of POA and aged OA from the cooking and vehicular sources.**

165 **Fig.1a** shows the mass spectra of aged HOA under different vehicle running conditions when EPA was  
166 0.6 days. The mass spectra of aged HOA emission from different vehicle running conditions under other  
167 various oxidation degrees are included in **Fig.S2**. All the aged HOA spectral profiles from different vehicle

168 running conditions showed a similar pattern, and the  $\theta$  angles among the mass spectra of aged HOA were  
 169 less than  $10^\circ$  at EPA 0.6 days (**Table 1**), suggesting a little difference between the mass spectra. The mass  
 170 spectra of aged HOA at 0.6 days were dominated by the ion series of  $C_nH^{+}_{2n+1}$  ( $m/z$  29, 43, 57, 71, 85...) and  
 171  $C_nH_{2n-1}^+$  ( $m/z$  41, 55, 69, 83...), resulting from less oxidized components such as saturated alkanes, alkenes.  
 172 As the highest proportion of ion fragments,  $m/z$  43 and 29 consisted of oxygen-containing ions like  $CHO^+$   
 173 and  $C_2H_3O^+$ , respectively, whose fractions were much larger than the hydrocarbon-like ion fragments at the  
 174 same mass integers. Besides, there were also abundant tracer ion fragments for SOA ( $m/z$  28 and  $m/z$  44).  
 175

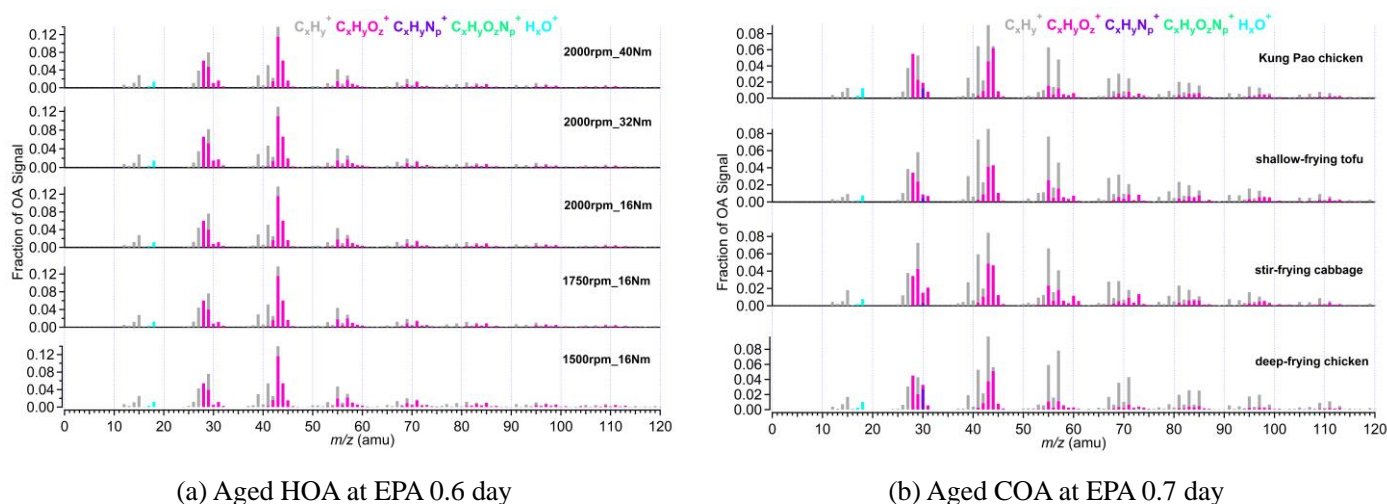


Fig.1. (a) The mass spectra of aged HOA emission from different vehicle running conditions at EPA 0.6 day; (b) The mass spectra of aged COA from four Chinese dishes at EPA 0.7 day. Five running conditions cover different speeds and torques, including 1500rpm\_16Nm, 1750rpm\_16Nm, 2000rpm\_16Nm, 2000rpm\_32Nm, and 2000rpm\_40Nm. Four dishes include deep-frying chicken, shallow-frying tofu, stir-frying cabbage, and Kung Pao chicken.

176  
 177 The mass spectra of aged COA at 0.7 days of EPA are presented in **Fig.1b**. Detailed mass spectra of  
 178 aged COA under other various oxidation degrees are included in **Fig.S3**. The similarity of aged COA among  
 179 different types of cooking was greater than that of aged HOA among different running conditions when the  
 180 EPA was at the same level. Except for the  $\theta$  angles of deep-frying chicken vs stir-frying cabbage ( $21^\circ$ ), and  
 181 deep-frying chicken vs shallow-frying tofu ( $19^\circ$ ), the  $\theta$  angles among other aged COA at EPA 0.7 day  
 182 exhibited good agreement ( $\theta < 15^\circ$ ) in mass spectra (**Table 1**). The mass spectra of cooking were dominated



183 by the similar ion series as those of vehicle, which were mostly m/z 28, m/z 29, m/z 41, m/z 43, m/z 44, m/z  
 184 55, m/z 57, m/z 67, and m/z 69. However, the major mass spectral differences between cooking and vehicle  
 185 were the abundance of m/z 41 and the ratio of oxygen-containing ions to hydrocarbon ions ( $C_xH_yO_z^+/C_xH_y^+$ ).  
 186 The four Chinese dishes had prominent peaks at m/z 41, m/z 43, and m/z 55 (generated from  $C_3H_5^+$  and  
 187  $C_3H_7^+$ ,  $C_4H_7^+$ ) which was qualitatively consistent with mass spectra of primary COA in other studies (Xu et  
 188 al., 2020). As described by He et al., 2010, the most abundant ion fragments at m/z 41 and m/z 55 from  
 189 primary Chinese cooking emissions associated with frying are resulting from unsaturated fatty acids

191 Table 1 The  $\theta$  angles among the mass spectra of (a) aged HOA at EPA 0.6 day and (b) aged COA at EPA 0.7 day

(a) $\theta$ angles	1500rpm_16Nm	1750rpm_16Nm	2000rpm_16Nm	2000rpm_32Nm	2000rpm_40Nm
1500rpm_16Nm	0	3	3	8	4
1750 rpm_16 Nm		0	0.1	5	3
2000 rpm_16 Nm			0	5	3
2000 rpm_32 Nm				0	4
2000 rpm_40 Nm					0

(b) $\theta$ angles	deep-frying chicken	stir-frying cabbage	shallow-frying tofu	Kung Pao chicken
deep-frying chicken	0	21	19	14
stir-frying cabbage		0	10	13
shallow-frying tofu			0	12
Kung Pao chicken				0

193  
 194 **Fig.2a** shows the mass spectra of aged HOA oxidation at different OH exposures under the same  
 195 vehicle running condition (2000rpm, 16Nm). The changes in mass spectra of aged HOA under different  
 196 conditions are provided in **Fig.S4**. It was worth noting that the source characteristics of vehicle POA were  
 197 uncertain due to its low concentration emitted from the engine in this study (**Table S4**). A related study has  
 198 found that the POA factor from vehicle emissions is similar to the HOA factor derived from environmental

199 datasets (Presto et al., 2014). Therefore, we used the average HOA spectrum derived from unconstrained  
 200 PMF analysis based on the ambient observations of Shanghai, Beijing, Dezhou, Shenzhen in China as an  
 201 alternative to the mass spectrum of vehicle POA, as shown in **Fig.2a** and **Fig.S4**. Detail observation  
 202 information of Shanghai, Dezhou, and Shenzhen referred to Zhu et al., 2021a. The observations in Beijing  
 203 have been given in Hu et al., 2017. The HOA spectrum was similar to that reported in Ng et al., 2011, which  
 204 has been widely used as traffic emission profiles. As the oxidation degree increased, the ion fragments  
 205 varied similarly with hydrocarbon-like ion fragments decreasing. The mass spectra at 2.9 days and 4.1 days  
 206 had very similar patterns with the most abundant signals at  $m/z$  28 and 44, respectively (**Fig.2** and **Fig.S4**),  
 207 which showed good consistency with the mass spectra of MO-OOA resolved from ambient datasets ( $\theta = 14^\circ$ ;  
 208 compared with MO-OOA obtained during the spring observations in Ng et al., 2011; Zhu et al., 2021b).  
 209 When EPA was 1.7 days, there were different mass spectra patterns, with dominant signals at  $m/z$  28 and  
 210  $m/z$  44, yet contained a large signal at  $m/z$  43, many similarities with the spectra of the ambient LO-OOA  
 211 (**Fig.2** and **Fig.S4**) (Hu et al., 2017; Zhu et al., 2021b). Oxidation degrees greatly affected the similarity of  
 212 mass spectra between POA and those of aged HOA. The mass spectra profile of HOA\_ambient displayed  
 213 poor agreement ( $\theta > 30^\circ$ ) with all aged HOA spectra profiles (**Tables S7**). Besides, the mass spectra under  
 214 the low oxidation degree (EPA was 0.6 day) was also poorly correlated with those mass spectra under the  
 215 high oxidation degree (EPA were 2.9 and 4.1 days) (**Table S7**).

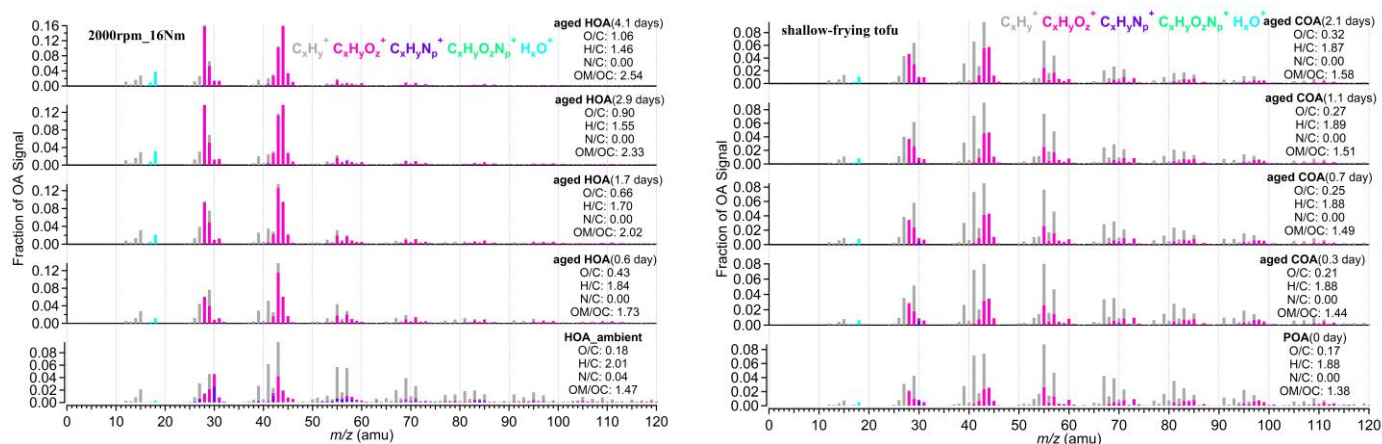


Fig.2. (a) The mass spectra of HOA and aged HOA oxidation under four different OH exposure at the same running

condition (2000rpm, 16Nm). (b) The mass spectra of primary COA and aged COA oxidation of different OH exposure for shallow-frying tofu. The EPA was obtained from off-line methods according to SO<sub>2</sub> decay shown in Table S3. The elemental compositions were estimated by the “improved-ambient” updated method (Canagaratna et al., 2015).

The mass spectra of primary COA and aged COA showed great inter-correlations ( $\theta < 15^\circ$ ), which were smaller than that of vehicle OA (**Table S8**). The spectra of aged COA derived herein displayed good consistency with those from cooking oils (Liu et al., 2018) (**Fig.2b** and **Fig.S5**). It should be noted that the fractions of m/z 28 and m/z 44 signals in aged COA were lower than those of aged HOA at the similar EPA. In addition, the aged COA had more hydrocarbon-like ions at the same mass integers than aged HOA.

All the above results imply that oxidation condition drives the variabilities in mass spectra of the vehicle OA. In contrast, cooking styles instead of oxidation conditions significantly affected the mass spectra of cooking OA. Here we concluded some possible explanations for these results. On one hand, under the same oxidation conditions and different emission conditions, the similarity among the mass spectra of vehicles was larger than that of cooking, which may be related to their precursors. Some studies have shown that the species and the proportion of gaseous organic matter emitted by different dishes are quite different (Wang et al., 2018). As described in the literature, alkanes and oxygenated volatile organic compounds (O-VOCs) contributed to over 97% of the total VOCs for fried food, and O-VOCs were the dominant contributors for Sichuan and Hunan cuisine where stir-frying is common (Wang et al., 2018). Different gaseous precursors cause distinctions in the particle phase SOA formation, which is reflected in the variations of AMS ion fragments between four dishes in our study. Compared to cooking, the precursors from vehicles are mainly hydrocarbons, and the difference in emissions under different running conditions is inapparent (Robinson et al., 2007). On the other hand, under the same emission conditions and different oxidation conditions, the similarity among the mass spectra of cooking sources is larger than that of vehicle sources, likely due to the oxidation pathway of precursors. As mentioned above, O-VOCs are important precursors of cooking sources, and their oxidation mechanisms are mostly alcohol/peroxide substitution

238 process. This conclusion was proved by a Van Krevelen diagram, showing that the cooking data gather  
239 around the slope of approximately -0.1 (Zhang et al., 2020), in agreement with that of heated oils OA (Liu et  
240 al., 2018). However, for vehicles, with the increase of oxidation degrees, the reaction pathways of  
241 hydrocarbon precursors varied diversely. In Van Krevelen space, the vehicle data fell along a line with a  
242 slope of -0.5 (**Fig.S6**), indicating oxidation processes involving the addition of both carboxylic acid and  
243 alcohol or peroxide functional groups without fragmentation and/or the addition of carboxylic acid  
244 functional groups with fragmentation.

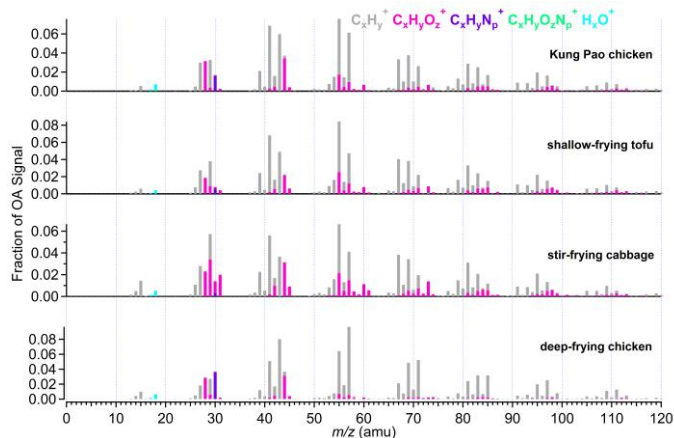
### 245 **3.2 Identification of the cooking and vehicular sources SOA mass spectra.**

246 Although the  $f_{44}$  (proportion of  $m/z$  44 in OA) of aged COA raised from 0.03 to 0.08 with oxidation  
247 increasing (**Fig.2b** and **Fig.S5**), the high abundance of  $m/z$  41, 55, and 57 in aged COA mass spectra for four  
248 dishes may be a sign that aged COA identified in this study is a mixture of POA and SOA. PMF analysis  
249 was performed on the high-resolution mass spectra to split SOA and POA factors from integrated primary  
250 COA and aged COA under each dish. Similarly, the same PMF procedure was also applied for vehicle aged  
251 datasets for each running condition. The choice of the PMF solution can be found in the supplement material  
252 (**Fig.S7-S10** and **Table S9-S10**; taken stir-frying cabbage for cooking, and 2000rpm\_32Nm for vehicle as an  
253 example).

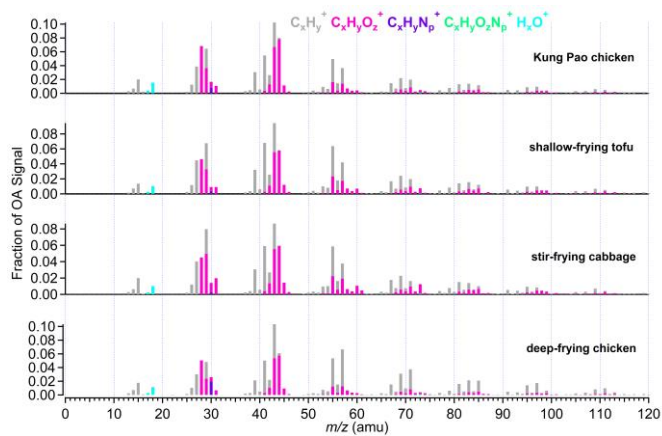
254 Some ions like  $m/z$  41, 55, 57, 43, 28, and 44 are typically used as tracers of OOA, COA, HOA,  
255 LO-OOA, and MO-OOA. **Fig.3** shows the high-resolution mass spectra of POA and SOA from four Chinese  
256 dishes and five vehicle running conditions. The cooking PMF POA of four Chinese dishes all showed  
257 obvious hydrocarbon-like signals at  $m/z$  41, 43, 55, 57, 67, and 69 with ion fragments of  $C_3H_5^+$ ,  $C_3H_7^+$ ,  
258  $C_4H_7^+$ ,  $C_4H_9^+$ ,  $C_5H_7^+$ , and  $C_5H_9^+$ , respectively. The fraction of  $m/z$  41 in cooking POA ranged from 0.051 to  
259 0.069. The prominent fraction of  $m/z$  43 ( $f_{43}=0.068\sim 0.083$ ), 55 ( $f_{55}=0.064\sim 0.084$ ), 57 ( $f_{57}=0.041\sim 0.097$ ), 67  
260 ( $f_{67}=0.021\sim 0.40$ ), 69 ( $f_{69}=0.034\sim 0.049$ ) were observed (Table S10). For mass spectra of cooking PMF SOA,

261 the oxidized ion fragments had higher signals than those of hydrocarbon-like ion fragments. The dominate  
262 signals existed at  $m/z$  28 ( $f_{28}=0.045\sim0.068$ ), 29 ( $f_{29}=0.048\sim0.080$ ), 41 ( $f_{41}=0.050\sim0.068$ ), 43  
263 ( $f_{43}=0.087\sim0.103$ ), 44 ( $f_{44}=0.058\sim0.080$ ), 55 ( $f_{55}=0.050\sim0.064$ ) (Table S11).

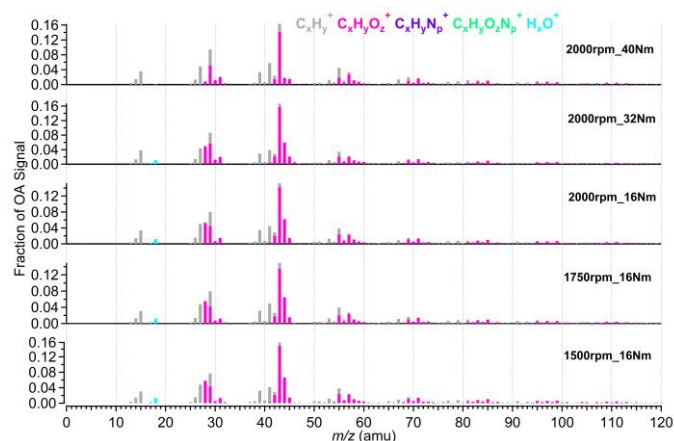
264 Different from the cooking, two-vehicle PMF SOA factors were derived from aged HOA, rather than  
265 integrated primary HOA and aged HOA datasets due to the low primary HOA emission (**Table S4**), as  
266 described in sect. 3.1. Unfortunately, vehicle PMF POA factor cannot be separated from aged HOA due to  
267 higher OH exposure. According to different O/C ratios, they were considered to be low oxidized vehicle  
268 SOA (LO-SOA) and more oxidized vehicle SOA (MO-SOA). As indicated in **Fig.3** and **Table S13**, the  
269 prominent  $m/z$  28 (average  $f_{28}=0.045$ ), 41 (average  $f_{41}=0.046$ ), 43 (average  $f_{43}=0.158$ ), 44 (average  
270  $f_{44}=0.054$ ), 55 (average  $f_{55}=0.039$ ), 57 (average  $f_{57}=0.027$ ) of vehicle PMF LO-SOA were comparable with  
271 those of cooking PMF SOA. The fraction of  $m/z$  43 of vehicle PMF LO-SOA was higher than that in  
272 cooking SOA by a factor of 2, which may be caused by the inability to separate vehicle PMF POA factor in  
273 the PMF analysis. The abundant  $m/z$  28 and 44 (mainly generated from  $\text{CO}_2^+$ ) are widely used as the  
274 ambient MO-OOA markers (Sun et al., 2018; Xu et al., 2017). We observed high fractions of  $m/z$  28  
275 ( $f_{28}=0.110\sim0.214$ ) and  $m/z$  44 ( $f_{44}=0.121\sim0.224$ ) in vehicle PMF MO-SOA (Table S13) and high O/C ratios  
276 (0.88~1.33), which were much higher than those of vehicle PMF LO-SOA (O/C=0.37~0.53) and cooking  
277 SOA (O/C=0.29~0.41).



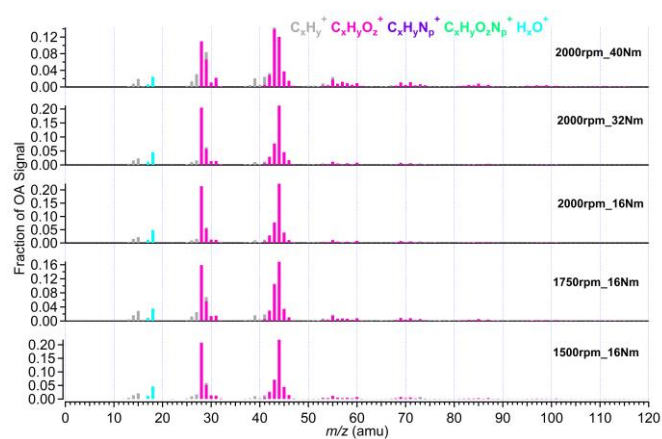
(a) Cooking PMF POA



(b) Cooking PMF SOA



(c) Vehicle PMF LO-SOA



(d) Vehicle PMF MO-SOA

Fig.3. The mass spectra of PMF POA and SOA from vehicle and cooking. PMF analysis was performed on the high-resolution mass spectra to split two factors (cooking POA and SOA) from aged COA and two SOA factors (vehicle LO-SOA and MO-SOA) from aged HOA, respectively.

279

280

281

282

283

284

285

286

287

Similarly, for the resolved SOA factors, the correlation of mass spectra among cooking groups under different cooking methods ( $\theta = 8\sim 21^\circ$ ) was worse than that of vehicle groups (vehicle PMF LO-SOA;  $\theta = 3\sim 19^\circ$ ) under different running conditions (**Table S15** and **Table S17**). The mass spectra of the PMF POA factors for deep-frying chicken exhibited poor agreement with those of stir-frying cabbage, Kung Pao chicken, and shallow-frying tofu (**Table S16**). In addition, we also found that the  $\theta$  angles between vehicle PMF LO-SOA and vehicle PMF MO-SOA under five GDI running conditions were ranged from  $36^\circ$  to  $50^\circ$  (**Fig.S11**), indicating that the mass spectra profiles of vehicle PMF LO-SOA are poor consistency with those of vehicle PMF MO-SOA, consistent with the changes in the mass spectra characteristics of vehicles, under

288 the same emission conditions and different oxidation conditions. Our results suggest that it is necessary to  
289 consider the cooking styles when constraining cooking and atmospheric oxidation conditions when  
290 constraining vehicle factors.

### 291 3.3 Application of established POA and SOA profile in ambient OA source apportionment.

292 The POA and SOA of the cooking as the primary and secondary spectrum constraints for ME-2 were  
293 obtained by averaging the high-resolution mass spectra datasets of the four dishes, which were identified  
294 from aged COA using the PMF model. Similarly, combining different GDI running conditions, the averaged  
295 vehicle LO-SOA and vehicle MO-SOA which were resolved based on aged HOA by using the PMF model  
296 were used as the inputting mass spectra profiles of vehicles for ME-2. The mass spectral profiles for cooking  
297 and vehicle as constraints in the ME-2 model are shown in **Fig.S12**.

298 The  $\theta$  angles between the mass spectral profiles from urban cooking and vehicular sources and ambient  
299 PMF-resolved factors were calculated and summarized in **Fig.4** and **Table S19**. The AMS mass spectra of  
300 ambient factors were obtained and averaged in Shanghai, Dezhou, Beijing, and Shenzhen in China (Hu et al.,  
301 2017; Zhu et al., 2021a). The  $\theta$  angles among ambient COA, HOA, LO-OOA, and MO-OOA factors and the  
302 cooking POA, SOA, and the vehicle LO-SOA, vehicle MO-SOA were ranged from 18° to 52° (**Fig.4**),  
303 suggesting that the cooking POA, cooking SOA, and the vehicle LO-SOA, vehicle MO-SOA can be used as  
304 source constraints for ME-2 in ambient air.

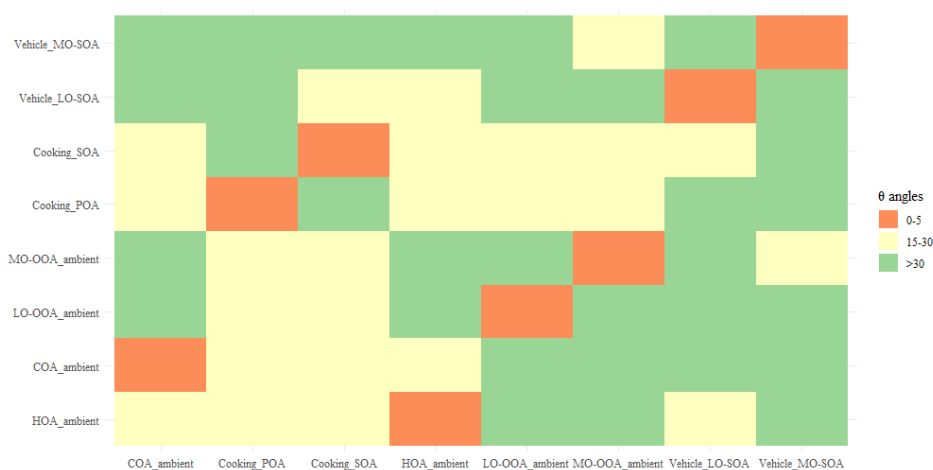


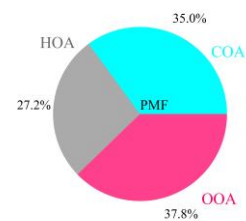
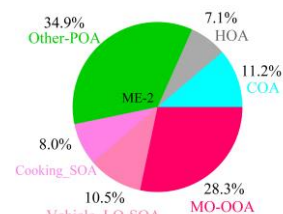
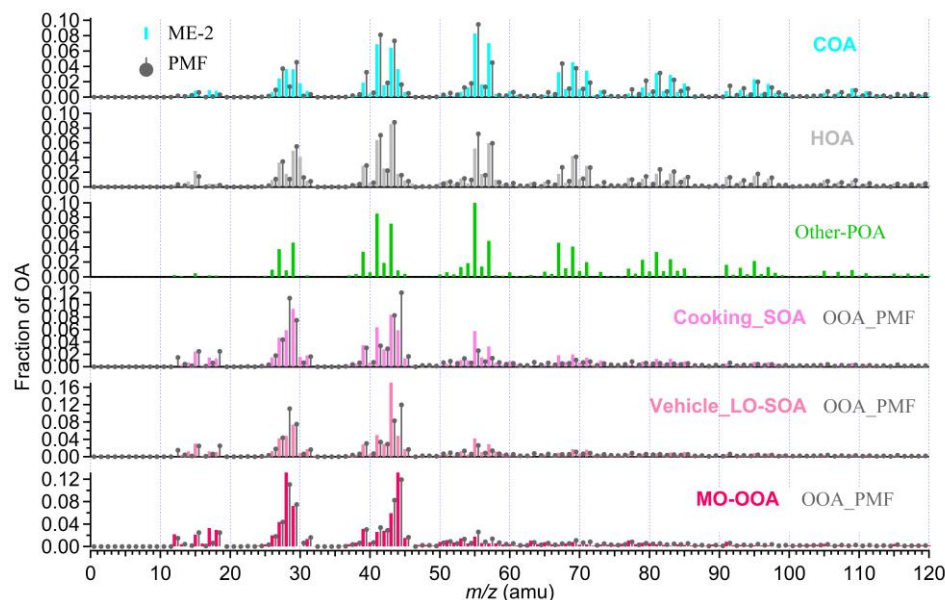
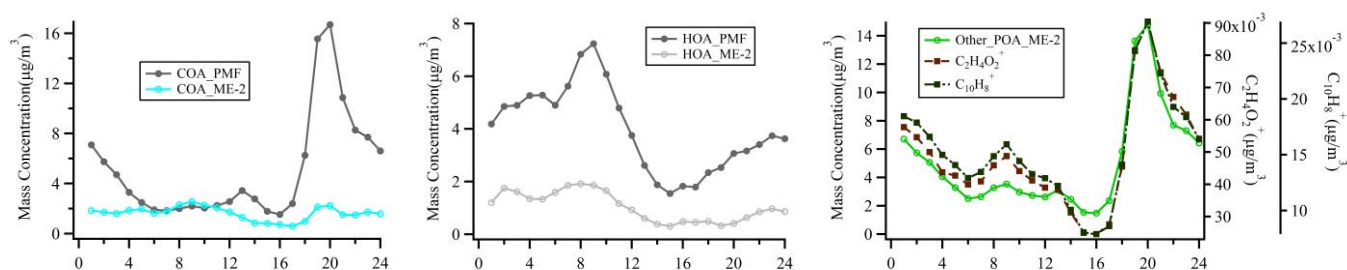
Fig.4. The  $\theta$  angles between ambient COA, HOA, LO-OOA, and MO-OOA factors and the cooking PMF POA, SOA, and the vehicle LO-SOA, MO-SOA. The  $\theta$  angle between two mass spectra is 0-5, 5-10, 10-15, 15-30, and  $> 30$  indicates excellent consistency, good consistency, many similarities, limited similarities, and poor consistency, respectively. The ambient COA, HOA, LO-OOA, and MO-OOA factors were averaged the resolved factors which performed on Shanghai, Dezhou, Beijing, and Shenzhen datasets (Hu et al., 2017; Zhu et al., 2021a).

305  
306       Considering the actual oxidation conditions, that is the concentration of OH radicals, and the lacking  
307 vehicle POA due to its low emission (**Table S4**), and the SOA spectra constraining reasonably, the cooking  
308 POA, cooking SOA, vehicle LO-SOA, and ambient HOA (instead of vehicle POA; derived from Beijing,  
309 Shenzhen, Dezhou, Shanghai ambient measurements) was finally selected as the input source spectra of  
310 ME-2. We further demonstrated the feasibility of input primary and secondary mass spectra for OA source  
311 apportionment in two field campaigns at the urban site of Shanghai in summer and winter. The ambient  
312 measurements in Shanghai were taken in situ at the same location as Zhu et al., 2021a, i.e., Shanghai  
313 Academy of Environmental Sciences (31.10°N, 121.25°E), a typical urban site in the Yangtze River Delta  
314 region from 23 August to 5 September 2016, and from 28 November 2016 to 12 December 2017 with  
315 HR-ToF-AMS at 4 min time resolution. For the tracers described below, the mass concentration of chemical  
316 compositions e.g., sulfate, nitrate, and ion-specified fragment were detected by HR-ToF-AMS, as shown in  
317 Zhu et al., 2021b. The detail measurements of black carbon (BC) and nitrogen oxides (NO<sub>x</sub>) can also be  
318 found in Zhu et al., 2021b. In general, the ME-2 source analysis was performed by constraining two primary  
319 OA factors (the cooking POA, HOA) and two secondary OA factors (the cooking SOA, the vehicle LO-SOA)  
320 with the fixed  $\alpha$ -value of 0.1 for HOA, 0.2 for cooking POA, 0.4 for vehicle LO-SOA and cooking SOA  
321 based on the same ambient OA datasets of the summer and winter observations in Shanghai. In ME-2  
322 solutions from 1 to 7 factors, we found the solution of 6 factors (i.e., COA, HOA, Other-POA, Cooking  
323 SOA, Vehicle LO-SOA) was most interpretable for the wintertime observations. For the 5 factors solution,  
324 in addition to the constraint four factors, factor 5 appeared to be mixed primary and secondary features.  
325 However, Other-POA split into two factors with similar profiles in seven factors solution (**Fig.S13**). Source



326 apportionment on OA datasets by using the unconstrained PMF model was also examined to compare with  
 327 ME-2 analysis. The choice for the optimal solution for the PMF model was presented in the supporting  
 328 information (**Fig.S14-S16** and **Table S20-S21**). Ambient PMF-resolved OA factors included POA factors  
 329 (i.e., HOA, COA), and SOA factors i.e., OOA (oxygenated OA) in the winter observations in Shanghai, on  
 330 average accounting for 27%, 35%, and 38% of OA mass. OOA resolved by PMF model did not separate into  
 331 two types of OOAs including LO-OOA and MO-OOA. Besides, we observed that HOA and COA profiles  
 332 (provided via PMF during the wintertime) contained high signals at the biomass burning tracer ion ( $m/z$  73),  
 333 and  $m/z$  91 (PAH-related  $m/z$ ), indicating that the mixing among HOA, COA, and other source emissions  
 334 (e.g., BBOA) (**Fig.5**).

335



338

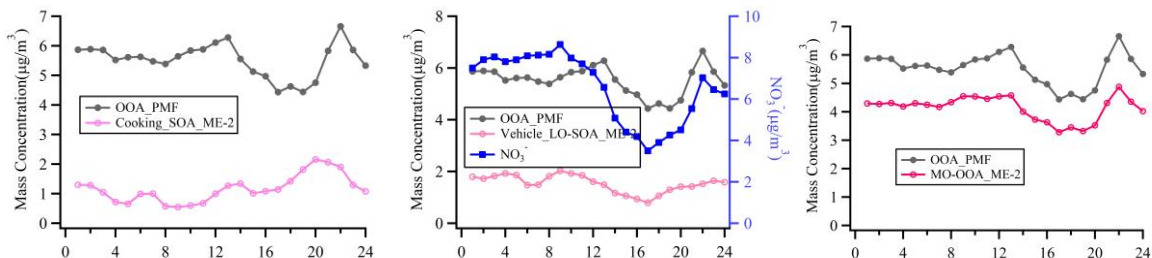


Fig.5. The comparison of the mass spectra, the diurnal variation, and fraction between ME-2 and PMF resolved factors during the wintertime in Shanghai. The black lines in the spectra and diurnal pattern are the results of PMF analysis of the actual atmosphere in Shanghai winter. The others correspond to the ME-2 source analysis results by using two primary OA factors (the cooking POA, ambient HOA) and two secondary OA factors (the cooking SOA, the vehicle LO-SOA) as constraints based on the same ambient OA datasets as the PMF model during the winter observations of Shanghai. Note that in the mass spectra and daily patterns, the OOA\_PMF factors which compared with vehicle LO-SOA and Cooking SOA respectively are the same, rather than the two resolved factors.

As shown in **Fig.5**, compared with PMF results, the proportions of HOA (7%) and COA (11%) obtained by source apportionment with ME-2 have significantly decreased to the expected value during the winter observation (Huang et al., 2020; Xu et al., 2020). As expected, other POA contributions were identified in the highly polluted season, correlated well with  $C_2H_4O_2^+$  and  $C_{10}H_8^+$ , which are well-known fragments from biomass burning and coal combustion emissions (**Fig.5**, **Fig.S17** and **Table S22**) (Alfarra et al., 2007; Duan et al., 2020; Hu et al., 2016a; Lee et al., 2010). The diurnal patterns of HOA\_PMF were consistent with HOA\_ME-2 during the winter observation, presenting low concentration during the daytime and high concentration at nighttime, likely due to the combined influence of boundary layer height and emissions from diesel vehicles during the nighttime. The temporal variation of two HOA factors showed a high correlation with NO<sub>x</sub> (Pearson  $r > 0.7$ ), suggesting two HOA factors are associated with vehicle emissions. Some variabilities existed between the diurnal cycle of COA\_PMF and COA\_ME-2. However, COA\_ME-2 correlated better with  $C_6H_{10}O^+$  than COA\_PMF, which was considered a fragment tracer mainly from cooking emissions (Ge et al., 2012; Hu et al., 2016a; Sun et al., 2011; Xu et al., 2016). For SOA factors, the sum of cooking SOA and vehicle LO-SOA had a high correlation with nitrate (Pearson  $r = 0.84$ ; **Fig.S17** and **Table S22**) and fragments of low-oxidizing substances ( $C_2H_3O^+$ ; Pearson  $r = 0.95$ ). In addition, we

362 noticed that the vehicle SOA analyzed by ME-2 exhibited consistency with the diurnal variation of nitrate,  
363 especially the reasonable morning peak (~09:00) retained, implying that vehicle SOA is well separated by  
364 using ME-2 in winter. MO-OOA resolved via ME-2 was characterized by prominent signal at m/z 28 and  
365 m/z 44, consistent with those in OOA identified by using PMF and in other studies (Duan et al., 2020; Kim  
366 et al., 2017). Meanwhile, there was a strong correlation between MO-OOA time series and sulfate (Pearson  $r$   
367 = 0.93), which was representative of regional aging species. Unfortunately, the SOA factor corresponding to  
368 other-POA (likely biomass burning OA) has not been resolved. Some studies have been found that OA  
369 emitted by biomass burning will be rapidly oxidized in the ambient atmosphere, and the BBOA in the fresh  
370 plume is mostly aged OA (Zhou et al., 2017). When the aged biomass burning OA is further oxidized, it is  
371 difficult to be identified the biomass burning SOA from mixed within OOA without constraining its SOA  
372 factor. Overall, ME-2 source analysis with the input of four source spectra profiles significantly improved  
373 the OA source apportionment during the wintertime. In comparing the ME-2 analysis results with only two  
374 POA factors constraining to that of the four factors constraining, the diurnal variations of HOA and COA  
375 obtained by constraining two primary sources were more consistent with those of the ME-2 constraint  
376 four-factor than PMF. However, OOA and POA were weakly separated, and the diurnal patterns of OOA  
377 were correlated with the case for the peak of other-POA during the evening (20:00~21:00) (**Fig.S18-S19**).  
378 These phenomena imply that the SOA factor constraint can be more environmentally meaningful factors to a  
379 certain extent.

380 For the source apportionment in summer with high oxidation conditions (**Fig.S20**), the fraction of COA  
381 reduced from 21% (PMF result) to 12% (ME-2 result). Moreover, the diurnal patterns of ME-2 SOA factors  
382 present more reasonable than PMF SOA factors. For example, the MO-OOA obtained based on ME-2  
383 analysis was in good agreement with the diurnal variation of  $O_x$  in summer. The Pearson  $r$  between  
384 MO-OOA\_ME-2 and  $CO_2^+$ (m/z 44), a marker of SOA was 0.95, higher than that of MO-OOA\_PMF (0.79),

385 which better reflects the characteristics of the MO-OOA factor in ME-2 (**Fig.S21** and **Table S23**). In general,  
386 the accurate source apportionment results have significantly indicated that the reliability source profiles of  
387 the primary and secondary of cooking and vehicles obtained in our study can be used as constraints for  
388 source apportionment of OA with ME-2 in various primary emissions or high oxidation conditions.

#### 389 4. Limitations and future work

390 POA emissions, and SOA formation in Go: PAM reactor from urban cooking and vehicular sources  
391 were explored. The aged COA had higher hydrocarbon ions than aged HOA in mass spectra. The spectra  
392 profiles of urban cooking and vehicular sources derived from the lab simulation were performed as  
393 constraints in ME-2 model. The OA source apportionment using ME-2 compared with unconstrained PMF  
394 based on the HR OA datasets in Shanghai validated the reasonable of the primary and secondary source  
395 profiles of cooking and vehicles. It is noted that the vehicle experiments were solely conducted under a  
396 single engine with gasoline, and the cooking experiment only related to limited cooking styles. The  
397 variations of VOCs in diesel and gasoline vehicle emissions may lead to differences in the SOA  
398 characteristics (Wang et al., 2020). The POA and gas-phase precursor emitted from another cooking style -  
399 meat charbroiling can also form a large amount of SOA after photochemical oxidation (Kaltsonoudis et al.,  
400 2017). More work needs to be done to explore the POA and SOA mass spectrometric characteristics of  
401 emissions from vehicles and cooking sources. In addition, SOA mass spectra were split from aged COA and  
402 aged HOA by using the PMF model, and therefore provided limited information on dynamic SOA mass  
403 spectra; we suggested that further studies control the oxidation conditions to obtain a set of dynamic pure  
404 SOA spectral profile. Especially, the absence of primary HOA due to low emissions of engine, and the  
405 inability to separate vehicle PMF POA from aged HOA in the PMF analysis were major limitations of this  
406 study. In addition to obtaining pure vehicle POA through source experiments, further work can apply ME-2  
407 model for constraining pure SOA profiles from experimental datasets to obtain the vehicle POA profiles.

408 Constraining many SOA factors could be over-constraining the ME-2 runs, which leads to factor mixing and  
409 reduces the number of factors. Therefore, SOA source spectra can only be appropriately and reasonably  
410 limited in ME-2 model. Besides, measurements of accurate tracers for all factors that resolved by PMF or  
411 ME-2 model should be conducted in future work to improve source apportionment verification. For example,  
412 we had to combine vehicle LO-SOA and cooking SOA as LO-OOA due to the lack of the measurement  
413 tracers for vehicle and cooking SOA factor, and then we analyzed the time series-correlation of LO-OOA  
414 with nitrate and other tracer ions. Due to the limitation of Go: PAM, dilution and high concentration of OH  
415 radicals without other inorganic aerosol seeds were adopted to measure and simulate atmospheric aging of  
416 aerosols. Thus, the possible atmospheric transformations and the reaction pathway are affected. In the future,  
417 it is still necessary to take further researches, for instance, use a quasi-atmospheric aerosol evolution study  
418 (QUALITY) chamber (Guo et al., 2020) to study the SOA formation under different actual oxidation  
419 conditions, like high/low NO<sub>x</sub> and so forth. Moreover, ambient datasets obtained from different sites and  
420 seasons need to be analyzed to validate the application of POA and SOA profiles of cooking and vehicles in  
421 this study, noting selecting a loose constraint via a value in SOA factors due to their high variability. Our  
422 research found that SOA from the urban cooking and vehicular sources contributed 19% and 35% of OA in  
423 the wintertime and summertime of Shanghai, implying the need to develop control measures to reduce  
424 emissions from cooking and vehicular sources in the future.

425  
426 **Nomenclature table**

Abbreviations	Description
OA	organic aerosol
POA	primary organic aerosol
SOA	secondary organic aerosol
HOA	hydrocarbon-like organic aerosol; associated with vehicle-related emissions in urban
COA	cooking organic aerosol
LO-OOA	low oxygenated organic aerosol

MO-OOA	more oxygenated organic aerosol
PMF	positive matrix factorization
ME-2	a multilinear engine
HR-ToF-AMS	high-resolution time-of-flight aerosol mass spectrometer
SMPS	scanning mobility particle sizers
Go: PAM	Gothenburg Potential Aerosol Mass reactor
VOCs	volatile organic compounds
SVOCs	semi-volatile organic compounds
IVOCs	intermediate volatile organic compounds
O-VOCs	oxygenated volatile organic compounds
$f_{28, 29, 41, 43, \dots}$	fraction of m/z 28, 29, 41, 43... in total organic aerosol
aged HOA	organic aerosols oxidized by Potential Aerosol Mass reactor in vehicle experiments
aged COA	organic aerosols oxidized by Potential Aerosol Mass reactor in cooking experiments
LO-SOA	low oxidized vehicle secondary organic aerosol
MO-SOA	more oxidized vehicle secondary organic aerosol

427

## 428 **Supporting information**

429 Schematic depiction of the simulation and measurement system (Figure S1); Details of the mass spectra of  
430 aged HOA and aged COA (Figures S2-S5; Table S5-S8); Van Krevelen diagram of POA, aged COA, and  
431 aged HOA (Figure S6); The choice for the PMF and ME-2 analysis (Figure S7-S10; Table S9-S10; Figure  
432 S13-S14; Table S20-S21); ME-2 source analysis during the summer observation in Shanghai (Figure S19);  
433 The time-series correlations of factors with external tracers (Figure S17-S18, S21; Table S22-S23);  
434 Experimental parameters (Table S1-S3); Mass spectra similarity analysis between mass spectra of ambient  
435 factor and mass spectral profiles for vehicle and cooking (Table S15-S19; Figure S11).

436 **Data availability.** The data provided in this paper can be obtained from the author upon request  
437 ([songguo@pku.edu.cn](mailto:songguo@pku.edu.cn)).

438 **Author contribution.** Wenfei Zhu, Zirui Zhang, Hui Wang, Ying Yu, Zheng Chen, Ruizhe Shen, Rui Tan,  
439 Kai Song, Kefan Liu, Rongzhi Tang, Yi Liu, Yuanju Li, Wenbin Zhang, and Zhou Zhang conducted the  
440 experiments. Wenfei Zhu, Zirui Zhang, Song Guo, and Min Hu analyzed the data. Shengrong Lou, Shijin

441 Shuai, Hongming Xu, Shuangde Li, Yunfa Chen, Francesco Canonaco, and Andre. S. H. Prévôt reviewed  
442 and commented on the paper. Wenfei Zhu and Song Guo wrote the paper.

443 **Competing interests.** The authors declare no competing financial interest.

444 **Acknowledgments.** This research was supported by the National Natural Science Foundation of China  
445 (51636003, 41977179, 91844301), Beijing Municipal Science and Technology Commission  
446 (Z201100008220011), the Natural Science Foundation of Beijing (8192022), the fellowship of China  
447 Postdoctoral Science Foundation (2020M680242), and the Open Research Fund of State Key Laboratory of  
448 Multiphase Complex Systems (No. MPCs-2021-D-12).

## 449 **References**

- 450 Alfarra, M.R., Prevot, A.S.H., Szidat, S., Sandradewi, J., Weimer, S., Lanz, V.A., Schreiber, D., Mohr, M., Baltensperger, U., 2007.  
451 Identification of the mass spectral signature of organic aerosols from wood burning emissions. *Environmental Science &*  
452 *Technology* 41, 5770-5777.
- 453 Budisulistiorini, S.H., Canagaratna, M.R., Croteau, P.L., Marth, W.J., Baumann, K., Edgerton, E.S., Shaw, S.L., Knipping, E.M.,  
454 Worsnop, D.R., Jayne, J.T., Gold, A., Surratt, J.D., 2013. Real-Time Continuous Characterization of Secondary Organic  
455 Aerosol Derived from Isoprene Epoxydiols in Downtown Atlanta, Georgia, Using the Aerodyne Aerosol Chemical Speciation  
456 Monitor. *Environmental Science & Technology* 47, 5686-5694.
- 457 Canagaratna, M., Jimenez, J., Kroll, J., Chen, Q., Kessler, S., Massoli, P., Hildebrandt Ruiz, L., Fortner, E., Williams, L., Wilson,  
458 K., 2015. Elemental ration measurements of organic compounds using aerosol mass spectrometry: characterization,  
459 improved calibration, and implications. *Atmos. Chem. Phys* 15, 253-272.
- 460 Canagaratna, M.R., Jayne, J.T., Jimenez, J.L., Allan, J.D., Alfarra, M.R., Zhang, Q., Onasch, T.B., Drewnick, F., Coe, H.,  
461 Middlebrook, A., Delia, A., Williams, L.R., Trimborn, A.M., Northway, M.J., DeCarlo, P.F., Kolb, C.E., Davidovits, P., Worsnop,  
462 D.R., 2007. Chemical and microphysical characterization of ambient aerosols with the aerodyne aerosol mass spectrometer.  
463 *Mass Spectrometry Reviews* 26, 185-222.
- 464 Canonaco, F., Crippa, M., Slowik, J.G., Baltensperger, U., Prevot, A.S.H., 2013. SoFi, an IGOR-based interface for the efficient  
465 use of the generalized multilinear engine (ME-2) for the source apportionment: ME-2 application to aerosol mass  
466 spectrometer data. *Atmospheric Measurement Techniques* 6, 3649-3661.
- 467 Collier, S., Zhou, S., Kuwayama, T., Forestieri, S., Brady, J., Zhang, M., Kleeman, M., Cappa, C., Bertram, T., Zhang, Q., 2015.  
468 Organic PM Emissions from Vehicles: Composition, O/C Ratio, and Dependence on PM Concentration. *Aerosol Science*  
469 *and Technology* 49, 86-97.
- 470 Crippa, M., Canonaco, F., Lanz, V.A., Aijala, M., Allan, J.D., Carbone, S., Capes, G., Ceburnis, D., Dall'Osto, M., Day, D.A.,  
471 DeCarlo, P.F., Ehn, M., Eriksson, A., Freney, E., Hildebrandt Ruiz, L., Hillamo, R., Jimenez, J.L., Junninen, H., Kiendler-Scharr,  
472 A., Kortelainen, A.M., Kulmala, M., Laaksonen, A., Mensah, A., Mohr, C., Nemitz, E., O'Dowd, C., Ovadnevaite, J., Pandis, S.N.,  
473 Petaja, T., Poulain, L., Saarikoski, S., Sellegri, K., Swietlicki, E., Tiitta, P., Worsnop, D.R., Baltensperger, U., Prevot, A.S.H., 2014.  
474 Organic aerosol components derived from 25 AMS data sets across Europe using a consistent ME-2 based source  
475 apportionment approach. *Atmospheric Chemistry and Physics* 14, 6159-6176.

476 Duan, J., Huang, R.-J., Li, Y., Chen, Q., Zheng, Y., Chen, Y., Lin, C., Ni, H., Wang, M., Ovadnevaite, J., Ceburnis, D., Chen, C.,  
477 Worsnop, D.R., Hoffmann, T., O'Dowd, C., Cao, J., 2020. Summertime and wintertime atmospheric processes of secondary  
478 aerosol in Beijing. *Atmospheric Chemistry and Physics* 20, 3793-3807.

479 Elser, M., Huang, R.-J., Wolf, R., Slowik, J.G., Wang, Q., Canonaco, F., Li, G., Bozzetti, C., Daellenbach, K.R., Huang, Y., Zhang,  
480 R., Li, Z., Cao, J., Baltensperger, U., El-Haddad, I., Prevot, A.S.H., 2016. New insights into PM<sub>2.5</sub> chemical composition and  
481 sources in two major cities in China during extreme haze events using aerosol mass spectrometry. *Atmospheric Chemistry  
482 and Physics* 16, 3207-3225.

483 Ge, X., Li, L., Chen, Y., Chen, H., Wu, D., Wang, J., Xie, X., Ge, S., Ye, Z., Xu, J., 2017. Aerosol characteristics and sources in  
484 Yangzhou, China resolved by offline aerosol mass spectrometry and other techniques. *Environmental Pollution* 225, 74-85.

485 Ge, X., Setyan, A., Sun, Y., Zhang, Q., 2012. Primary and secondary organic aerosols in Fresno, California during wintertime:  
486 Results from high resolution aerosol mass spectrometry. *Journal of Geophysical Research - Atmospheres* 117.

487 Gentner, D.R., Harley, R.A., Miller, A.M., Goldstein, A.H., 2009. Diurnal and Seasonal Variability of Gasoline-Related Volatile  
488 Organic Compound Emissions in Riverside, California. *Environmental Science & Technology* 43, 4247-4252.

489 Guo, S., Hu, M., Guo, Q., Zhang, X., Zheng, M., Zheng, J., Chang, C.C., Schauer, J.J., Zhang, R., 2012. Primary Sources and  
490 Secondary Formation of Organic Aerosols in Beijing, China. *Environmental Science & Technology* 46, 9846-9853.

491 Guo, S., Hu, M., Peng, J., Wu, Z., Zamora, M.L., Shang, D., Du, Z., Zheng, J., Fang, X., Tang, R., Wu, Y., Zeng, L., Shuai, S.,  
492 Zhang, W., Wang, Y., Ji, Y., Li, Y., Zhang, A.L., Wang, W., Zhang, F., Zhao, J., Gong, X., Wang, C., Molina, M.J., Zhang, R., 2020.  
493 Remarkable nucleation and growth of ultrafine particles from vehicular exhaust. *Proceedings of the National Academy of  
494 Sciences of the United States of America* 117, 3427-3432.

495 Guo, S., Hu, M., Zamora, M.L., Peng, J., Shang, D., Zheng, J., Du, Z., Wu, Z., Shao, M., Zeng, L., Molina, M.J., Zhang, R., 2014.  
496 Elucidating severe urban haze formation in China. *Proceedings of the National Academy of Sciences of the United States of  
497 America* 111, 17373-17378.

498 He, L.Y., Huang, X.F., Xue, L., Hu, M., Lin, Y., Zheng, J., Zhang, R., Zhang, Y.H., 2011. Submicron aerosol analysis and organic  
499 source apportionment in an urban atmosphere in Pearl River Delta of China using high-resolution aerosol mass  
500 spectrometry. *Journal of Geophysical Research Atmospheres* 116, -.

501 He, L.Y., Lin, Y., Huang, X.F., Guo, S., Xue, L., Su, Q., Hu, M., Luan, S.J., Zhang, Y.H., 2010. Characterization of high-resolution  
502 aerosol mass spectra of primary organic aerosol emissions from Chinese cooking and biomass burning. *Atmospheric  
503 Chemistry and Physics* 10, 11535-11543.

504 Hu, W., Hu, M., Hu, W., Jimenez, J.L., Yuan, B., Chen, W., Wang, M., Wu, Y., Chen, C., Wang, Z., 2016a. Chemical composition,  
505 sources, and aging process of submicron aerosols in Beijing: Contrast between summer and winter. *Journal of Geophysical  
506 Research Atmospheres* 121, 1955-1977.

507 Hu, W., Hu, M., Hu, W.W., Zheng, J., Chen, C., Wu, Y., Guo, S., 2017. Seasonal variations in high time-resolved chemical  
508 compositions, sources, and evolution of atmospheric submicron aerosols in the megacity Beijing. *Atmospheric Chemistry &  
509 Physics* 17, 9979-10000.

510 Hu, W., Palm, B.B., Day, D.A., Campuzano-Jost, P., Krechmer, J.E., Peng, Z., de Sa, S.S., Martin, S.T., Alexander, M.L.,  
511 Baumann, K., Hacker, L., Kiendler-Scharr, A., Koss, A.R., de Gouw, J.A., Goldstein, A.H., Seco, R., Sjostedt, S.J., Park, J.-H.,  
512 Guenther, A.B., Kim, S., Canonaco, F., Prevot, A.S.H., Brune, W.H., Jimenez, J.L., 2016b. Volatility and lifetime against OH  
513 heterogeneous reaction of ambient isoprene-epoxydiols-derived secondary organic aerosol (IEPOX-SOA). *Atmospheric  
514 Chemistry and Physics* 16, 11563-11580.

515 Huang, R.-J., He, Y., Duan, J., Li, Y., Chen, Q., Zheng, Y., Chen, Y., Hu, W., Lin, C., Ni, H., Dai, W., Cao, J., Wu, Y., Zhang, R., Xu,  
516 W., Ovadnevaite, J., Ceburnis, D., Hoffmann, T., O'Dowd, C.D., 2020. Contrasting sources and processes of particulate  
517 species in haze days with low and high relative humidity in wintertime Beijing. *Atmospheric Chemistry and Physics* 20,  
518 9101-9114.

519 Huang, X.F., He, L.Y., Hu, M., Canagaratna, M.R., Kroll, J.H., Ng, N.L., Zhang, Y.H., Lin, Y., Xue, L., Sun, T.L., 2011.  
520 Characterization of submicron aerosols at a rural site in Pearl River Delta of China using an Aerodyne High-Resolution  
521 Aerosol Mass Spectrometer. *Atmospheric Chemistry & Physics* 11, 1865-1877.



522 Kaltsonoudis, C., Kostenidou, E., Louvaris, E., Psichoudaki, M., Tsiligiannis, E., Florou, K., Liangou, A., Pandis, S.N., 2017.  
523 Characterization of fresh and aged organic aerosol emissions from meat charbroiling. *Atmospheric Chemistry and Physics*  
524 17, 7143-7155.

525 Katragadda, H.R., Fullana, A., Sidhu, S., Carbonell-Barrachina, A.A., 2010. Emissions of volatile aldehydes from heated  
526 cooking oils. *Food Chemistry* 120, 59-65.

527 Kim, H., Zhang, Q., Bae, G.-N., Kim, J.Y., Lee, S.B., 2017. Sources and atmospheric processing of winter aerosols in Seoul,  
528 Korea: insights from real-time measurements using a high-resolution aerosol mass spectrometer. *Atmospheric Chemistry*  
529 *and Physics* 17, 2009-2033.

530 Klein, F., Platt, S.M., Farren, N.J., Detournay, A., Bruns, E.A., Bozzetti, C., Daellenbach, K.R., Kilic, D., Kumar, N.K., Pieber, S.M.,  
531 Slowik, J.G., Temime-Roussel, B., Marchand, N., Hamilton, J.F., Baltensperger, U., Prevot, A.S.H., El Haddad, I., 2016.  
532 Characterization of Gas-Phase Organics Using Proton Transfer Reaction Time-of-Flight Mass Spectrometry: Cooking  
533 Emissions. *Environmental Science & Technology* 50, 1243-1250.

534 Kostenidou, E., Lee, B.-H., Engelhart, G.J., Pierce, J.R., Pandis, S.N., 2009. Mass Spectra Deconvolution of Low, Medium, and  
535 High Volatility Biogenic Secondary Organic Aerosol. *Environmental Science & Technology* 43, 4884-4889.

536 Kroll, J.H., Smith, J.D., Worsnop, D.R., Wilson, K.R., 2012. Characterisation of lightly oxidised organic aerosol formed from  
537 the photochemical aging of diesel exhaust particles. *Environmental Chemistry* 9, 211-220.

538 Lee, T., Sullivan, A.P., Mack, L., Jimenez, J.L., Kreidenweis, S.M., Onasch, T.B., Worsnop, D.R., Malm, W., Wold, C.E., Hao,  
539 W.M., Collett, J.L., Jr., 2010. Chemical Smoke Marker Emissions During Flaming and Smoldering Phases of Laboratory Open  
540 Burning of Wildland Fuels. *Aerosol Science and Technology* 44, I-V.

541 Li, J., Liu, Q., Li, Y., Liu, T., Huang, D., Zheng, J., Zhu, W., Hu, M., Wu, Y., Lou, S., Hallquist, A.M., Hallquist, M., Chan, C.K.,  
542 Canonaco, F., Prevot, A.S.H., Fung, J.C.H., Lau, A.K.H., Yu, J.Z., 2019. Characterization of Aerosol Aging Potentials at  
543 Suburban Sites in Northern and Southern China Utilizing a Potential Aerosol Mass (Go:PAM) Reactor and an Aerosol Mass  
544 Spectrometer. *Journal of Geophysical Research-Atmospheres* 124, 5629-5649.

545 Li, Y.J., Sun, Y., Zhang, Q., Li, X., Li, M., Zhou, Z., Chan, C.K., 2017. Real-time chemical characterization of atmospheric  
546 particulate matter in China: A review. *Atmospheric Environment* 158, 270-304.

547 Liu, T., Li, Z., Chan, M., Chan, C.K., 2017. Formation of secondary organic aerosols from gas-phase emissions of heated  
548 cooking oils. *Atmospheric Chemistry and Physics* 17, 7333-7344.

549 Liu, T., Wang, Z., Wang, X., Chan, C.K., 2018. Primary and secondary organic aerosol from heated cooking oil emissions.  
550 *Atmospheric Chemistry and Physics* 18, 11363-11374.

551 Louvaris, E.E., Karnezi, E., Kostenidou, E., Kaltsonoudis, C., Pandis, S.N., 2017. Estimation of the volatility distribution of  
552 organic aerosol combining thermodenuder and isothermal dilution measurements. *Atmospheric Measurement Techniques*  
553 10, 3909-3918.

554 Mohr, C., DeCarlo, P.F., Heringa, M.F., Chirico, R., Slowik, J.G., Richter, R., Reche, C., Alastuey, A., Querol, X., Seco, R.,  
555 Penuelas, J., Jimenez, J.L., Crippa, M., Zimmermann, R., Baltensperger, U., Prevot, A.S.H., 2012. Identification and  
556 quantification of organic aerosol from cooking and other sources in Barcelona using aerosol mass spectrometer data.  
557 *Atmospheric Chemistry and Physics* 12, 1649-1665.

558 Ng, N.L., Canagaratna, M.R., Jimenez, J.L., Zhang, Q., Ulbrich, I.M., Worsnop, D.R., 2011. Real-Time Methods for Estimating  
559 Organic Component Mass Concentrations from Aerosol Mass Spectrometer Data. *Environmental Science & Technology* 45,  
560 910-916.

561 Paatero, P., 1999. The multilinear engine - A table-driven, least squares program for solving multilinear problems,  
562 including the n-way parallel factor analysis model. *Journal of Computational and Graphical Statistics* 8, 854-888.

563 Paatero, P., Hopke, P.K., 2003. Discarding or downweighting high-noise variables in factor analytic models. *Analytica*  
564 *Chimica Acta* 490, 277-289.

565 Peng, Z., Day, D.A., Ortega, A.M., Palm, B.B., Hu, W., Stark, H., Li, R., Tsigaridis, K., Brune, W.H., Jimenez, J.L., 2016. Non-OH  
566 chemistry in oxidation flow reactors for the study of atmospheric chemistry systematically examined by modeling.  
567 *Atmospheric Chemistry and Physics* 16, 4283-4305.

568 Presto, A.A., Gordon, T.D., Robinson, A.L., 2014. Primary to secondary organic aerosol: evolution of organic emissions from  
569 mobile combustion sources. *Atmospheric Chemistry and Physics* 14, 5015-5036.

570 Qin, Y.M., Tan, H.B., Li, Y.J., Schurman, M.I., Li, F., Canonaco, F., Prevot, A.S.H., Chan, C.K., 2017. Impacts of traffic emissions  
571 on atmospheric particulate nitrate and organics at a downwind site on the periphery of Guangzhou, China. *Atmospheric*  
572 *Chemistry and Physics* 17, 10245-10258.

573 Reyes-Villegas, E., Green, D.C., Priestman, M., Canonaco, F., Coe, H., Prevot, A.S.H., Allan, J.D., 2016. Organic aerosol source  
574 apportionment in London 2013 with ME-2: exploring the solution space with annual and seasonal analysis. *Atmospheric*  
575 *Chemistry and Physics* 16, 15545-15559.

576 Robinson, A.L., Donahue, N.M., Shrivastava, M.K., Weitkamp, E.A., Sage, A.M., Grieshop, A.P., Lane, T.E., Pierce, J.R., Pandis,  
577 S.N., 2007. Rethinking organic aerosols: Semivolatile emissions and photochemical aging. *Science* 315, 1259-1262.

578 Schauer, J.J., Kleeman, M.J., Cass, G.R., Simoneit, B.R.T., 2002. Measurement of emissions from air pollution sources. 4.  
579 C-1-C-27 organic compounds from cooking with seed oils. *Environmental Science & Technology* 36, 567-575.

580 Sun, J., Zhang, Q., Canagaratna, M.R., Zhang, Y., Ng, N.L., Sun, Y., Jayne, J.T., Zhang, X., Zhang, X., Worsnop, D.R., 2010.  
581 Highly time- and size-resolved characterization of submicron aerosol particles in Beijing using an Aerodyne Aerosol Mass  
582 Spectrometer. *Atmospheric Environment* 44, 131-140.

583 Sun, Y., Du, W., Fu, P., Wang, Q., Li, J., Ge, X., Zhang, Q., Zhu, C., Ren, L., Xu, W., 2016. Primary and secondary aerosols in  
584 Beijing in winter: sources, variations and processes. *Atmospheric Chemistry & Physics* 16, 1-41.

585 Sun, Y., Jiang, Q., Wang, Z., Fu, P., Li, J., Yang, T., Yin, Y., 2014. Investigation of the sources and evolution processes of  
586 severe haze pollution in Beijing in January 2013. *Journal of Geophysical Research Atmospheres* 119, 4380-4398.

587 Sun, Y., Xu, W., Zhang, Q., Jiang, Q., Canonaco, F., Prévôt, A.S., Fu, P., Li, J., Jayne, J., Worsnop, D.R., 2018. Source  
588 apportionment of organic aerosol from two-year highly time-resolved measurements by an aerosol chemical speciation  
589 monitor in Beijing, China. *Atmospheric Chemistry and Physics Discussions*, 1-33.

590 Sun, Y.L., Zhang, Q., Schwab, J.J., Demerjian, K.L., Chen, W.N., Bae, M.S., Hung, H.M., Hogrefe, O., Frank, B., Rattigan, O.V.,  
591 Lin, Y.C., 2011. Characterization of the sources and processes of organic and inorganic aerosols in New York city with a  
592 high-resolution time-of-flight aerosol mass spectrometer. *Atmospheric Chemistry and Physics* 11, 1581-1602.

593 Tang, R.Z., Lu, Q.Y., Guo, S., Wang, H., Song, K., Yu, Y., Tan, R., Liu, K.F., Shen, R.Z., Chen, S.Y., Zeng, L.M., Jorga, S.D., Zhang,  
594 Z., Zhang, W.B., Shuai, S.J., Robinson, A.L., 2021. Measurement report: Distinct emissions and volatility distribution of  
595 intermediate-volatility organic compounds from on-road Chinese gasoline vehicles: implication of high secondary organic  
596 aerosol formation potential. *Atmospheric Chemistry and Physics* 21, 2569-2583.

597 Ulbrich, I., Canagaratna, M., Zhang, Q., Worsnop, D., Jimenez, J., 2009. Interpretation of organic components from positive  
598 matrix factorization of aerosol mass spectrometric data. *Atmospheric Chemistry & Physics* 9.

599 Wang, H., Guo, S., Yu, Y., Shen, R., Zhu, W., Tang, R., Tan, R., Liu, K., Song, K., Zhang, W., Zhang, Z., Shuai, S., Xu, H., Zheng,  
600 J., Chen, S., Li, S., Zeng, L., Wu, Z., 2021. Secondary aerosol formation from a Chinese gasoline vehicle: Impacts of fuel (E10,  
601 gasoline) and driving conditions (idling, cruising). *The Science of the total environment* 795, 148809-148809.

602 Wang, H., Xiang, Z., Wang, L., Jing, S., Lou, S., Tao, S., Liu, J., Yu, M., Li, L., Lin, L., Chen, Y., Wiedensohler, A., Chen, C., 2018.  
603 Emissions of volatile organic compounds (VOCs) from cooking and their speciation: A case study for Shanghai with  
604 implications for China. *Science of the Total Environment* 621, 1300-1309.

605 Wang, J., Ge, X., Chen, Y., Shen, Y., Zhang, Q., Sun, Y., Xu, J., Ge, S., Yu, H., Chen, M., 2016. Highly time-resolved urban  
606 aerosol characteristics during springtime in Yangtze River Delta, China: insights from soot particle aerosol mass  
607 spectrometry. *Atmospheric Chemistry and Physics* 16, 9109-9127.

608 Wang, M., Li, S., Zhu, R., Zhang, R., Zu, L., Wang, Y., Bao, X., 2020. On-road tailpipe emission characteristics and ozone  
609 formation potentials of VOCs from gasoline, diesel and liquefied petroleum gas fueled vehicles. *Atmospheric Environment*  
610 223.

611 Wang, Y.C., Huang, R.J., Ni, H.Y., Chen, Y., Wang, Q.Y., Li, G.H., Tie, X.X., Shen, Z.X., Huang, Y., Liu, S.X., Dong, W.M., Xue, P.,  
612 Frohlich, R., Canonaco, F., Elser, M., Daellenbach, K.R., Bozzetti, C., Haddad, I.E., Prevot, A.S.H., Canagaratna, M.R., Worsnop,

613 D.R., Cao, J.J., 2017. Chemical composition, sources and secondary processes of aerosols in Baoji city of northwest China.  
614 *Atmospheric Environment* 158, 128-137.

615 Watne, A.K., Psichoudaki, M., Ljungstrom, E., Le Breton, M., Hallquist, M., Jerksjo, M., Fallgren, H., Jutterstrom, S., Hallquist,  
616 A.M., 2018. Fresh and Oxidized Emissions from In-Use Transit Buses Running on Diesel, Biodiesel, and CNG. *Environmental*  
617 *Science & Technology* 52, 7720-7728.

618 Xu, J., Shi, J., Zhang, Q., Ge, X., Canonaco, F., Prévôt, A.S., Vonwiller, M., Szidat, S., Ge, J., Ma, J., 2016. Wintertime organic  
619 and inorganic aerosols in Lanzhou, China: sources, processes, and comparison with the results during summer.  
620 *Atmospheric Chemistry and Physics* 16, 14937-14957.

621 Xu, W., Han, T., Wei, D., Wang, Q., Chen, C., Jian, Z., Zhang, Y., Jie, L., Fu, P., Wang, Z., 2017. Effects of Aqueous-phase and  
622 Photochemical Processing on Secondary Organic Aerosol Formation and Evolution in Beijing, China. *Environmental*  
623 *Science & Technology* 51, 762.

624 Xu, W., He, Y., Qiu, Y., Chen, C., Xie, C., Lei, L., Li, Z., Sun, J., Li, J., Fu, P., Wang, Z., Worsnop, D., Sun, Y., 2020. Mass spectral  
625 characterization of primary emissions and implications in source apportionment of organic aerosol. *Atmospheric*  
626 *Measurement Techniques* 13, 3205-3219.

627 Ying, Y.A.B., Hui, W.A., A, T.W., Kai, S.A., A, T.T., A, Z.W., C, Y.G., A, H.D., A, S.C., D, L.Z.A.B., 2020. Elucidating the importance  
628 of semi-volatile organic compounds to secondary organic aerosol formation at a regional site during the EXPLORE-YRD  
629 campaign - ScienceDirect. *Atmospheric Environment*.

630 Yu, Y., Wang, H., Wang, T.T., Song, K., Tan, T.Y., Wan, Z.C., Gao, Y.Q., Dong, H.B., Chen, S.Y., Zeng, L.M., Hu, M., Wang, H.L.,  
631 Lou, S.R., Zhu, W.F., Guo, S., 2021. Elucidating the importance of semi-volatile organic compounds to secondary organic  
632 aerosol formation at a regional site during the EXPLORE-YRD campaign. *Atmospheric Environment* 246.

633 Zhang, Q., Jimenez, J.L., Canagaratna, M.R., Ulbrich, I.M., Ng, N.L., Worsnop, D.R., Sun, Y., 2011. Understanding atmospheric  
634 organic aerosols via factor analysis of aerosol mass spectrometry: a review. *Analytical & Bioanalytical Chemistry* 401,  
635 3045-3067.

636 Zhang, X., Zhang, Y., Sun, J., Yu, Y., Canonaco, F., Prevot, A.S.H., Li, G., 2017a. Chemical characterization of submicron  
637 aerosol particles during wintertime in a northwest city of China using an Aerodyne aerosol mass spectrometry.  
638 *Environmental Pollution* 222, 567-582.

639 Zhang, Y., Tang, L., Sun, Y., Favez, O., Canonaco, F., Albinet, A., Couvidat, F., Liu, D., Jayne, J.T., Wang, Z., Croteau, P.L.,  
640 Canagaratna, M.R., Zhou, H.-c., Prevot, A.S.H., Worsnop, D.R., 2017b. Limited formation of isoprene epoxydiols-derived  
641 secondary organic aerosol under NO<sub>x</sub>-rich environments in Eastern China. *Geophysical Research Letters* 44, 2035-2043.

642 Zhang, Y.J., Tang, L.L., Wang, Z., Yu, H.X., Sun, Y.L., Liu, D., Qin, W., Zhang, H.L., Zhou, H.C., 2014. Insights into  
643 characteristics, sources and evolution of submicron aerosols during harvest seasons in Yangtze River Delta (YRD) region,  
644 China. *Atmospheric Chemistry & Physics* 14, 9109-9154.

645 Zhang, Z., Zhu, W., Hu, M., Wang, H., Chen, Z., Shen, R., Yu, Y., Tan, R., Guo, S., 2020. Secondary Organic Aerosol from  
646 Typical Chinese Domestic Cooking Emissions. *Environmental Science & Technology Letters*.

647 Zhou, S., Collier, S., Jaffe, D.A., Briggs, N.L., Hee, J., Sedlacek, A.J., III, Kleinman, L., Onasch, T.B., Zhang, Q., 2017. Regional  
648 influence of wildfires on aerosol chemistry in the western US and insights into atmospheric aging of biomass burning  
649 organic aerosol. *Atmospheric Chemistry and Physics* 17, 2477-2493.

650 Zhou, W., Wang, Q., Zhao, X., Xu, W., Chen, C., Du, W., Zhao, J., Canonaco, F., Prevot, A.S.H., Fu, P., Wang, Z., Worsnop, D.R.,  
651 Sun, Y., 2018. Characterization and source apportionment of organic aerosol at 260 m on a meteorological tower in Beijing,  
652 China. *Atmospheric Chemistry and Physics* 18, 3951-3968.

653 Zhu, Q., Huang, X.-F., Cao, L.-M., Wei, L.-T., Zhang, B., He, L.-Y., Elser, M., Canonaco, F., Slowik, J.G., Bozzetti, C., El-Haddad,  
654 I., Prevot, A.S.H., 2018. Improved source apportionment of organic aerosols in complex urban air pollution using the  
655 multilinear engine (ME-2). *Atmospheric Measurement Techniques* 11, 1049-1060.

656 Zhu, W., Guo, S., Lou, S., Wang, H., Yu, Y., Xu, W., Liu, Y., Cheng, Z., Huang, X., He, L., Zeng, L., Chen, S., Hu, M., 2021a. A  
657 novel algorithm to determine the scattering coefficient of ambient organic aerosols. *Environmental Pollution* 270.

658 Zhu, W., Zhou, M., Cheng, Z., Yan, N., Huang, C., Qiao, L., Wang, H., Liu, Y., Lou, S., Guo, S., 2021b. Seasonal variation of  
659 aerosol compositions in Shanghai, China: Insights from particle aerosol mass spectrometer observations. *The Science of*  
660 *the total environment* 771, 144948-144948.

661